intensity of tens of GW cm^{-2} at 800 nm (*30*, *31*). The vertically aligned ZnO wires exhibit significant enhancement of optical nonlinearities: The 2PA coefficient (α_2) is greater than 10^3 cm GW^{-1} (*32*, *33*), and the wires show strong 3PA at high excitation intensities (*34*). The increased multiphoton absorption has been attributed to the local-field enhancement because of the surface states and the interaction between the aligned wire facets (*32*). With the 2PA coefficient of $\alpha_2 \sim 4 \times 10^3$ cm GW^{-1}, the effective penetration depth at our $I = 75$ GW cm^{-2} is ~33 nm. However, because of saturation this length can reach micrometers.

26. J. Tang, D.-S. Yang, A. H. Zewail, *J. Phys. Chem. C* **111**, 8957 (2007).
27. M. H. Huang *et al.*, *Science* **292**, 1897 (2001).
28. We note that the promptness of the intensity and width change (*14*) comes from the direct cascade of optical (and acoustic) phonon generation, which in this case amounts to ~20 for 3PA. Because the initial excitation induces in-plane movements of atoms, the intensity of ($\bar{1}14$) and ($1\bar{1}4$) spots should decrease before that of the (006), as observed experimentally.
29. B. E. Warren, *X-Ray Diffraction* (Dover, New York, 1990).
30. J. He, Y. Qu, H. Li, J. Mi, W. Ji, *Opt. Express* **13**, 9235 (2005).
31. B. Gu, J. He, W. Ji, H.-T. Wang, *J. Appl. Phys.* **103**, 073105 (2008).
32. H. W. Lee *et al.*, *Chem. Phys. Lett.* **447**, 86 (2007).
33. S. Xiao *et al.*, *Chin. Phys. B* **17**, 1291 (2008).
34. C. F. Zhang, Z. W. Dong, G. J. You, S. X. Qian, H. Deng, *Opt. Lett.* **31**, 3345 (2006).
35. This work was supported by the NSF and the Air Force Office of Scientific Research in the Gordon and Betty Moore Center at Caltech. We wish to thank Z. L. Wang for providing the samples, which were made by P. Fei and S. Xu, and K. Xu for the help with the SEM measurement in J. R. Heath's laboratory at Caltech.

Chondrulelike Objects in Short-Period Comet 81P/Wild 2

Tomoki Nakamura,[1]* Takaaki Noguchi,[2] Akira Tsuchiyama,[3] Takayuki Ushikubo,[4] Noriko T. Kita,[4] John W. Valley,[4] Michael E. Zolensky,[5] Yuki Kakazu,[1] Kanako Sakamoto,[1] Etsuko Mashio,[3] Kentaro Uesugi,[6] Tsukasa Nakano[7]

The Stardust spacecraft returned cometary samples that contain crystalline material, but the origin of the material is not yet well understood. We found four crystalline particles from comet 81P/Wild 2 that were apparently formed by flash-melting at a high temperature and are texturally, mineralogically, and compositionally similar to chondrules. Chondrules are submillimeter particles that dominate chondrites and are believed to have formed in the inner solar nebula. The comet particles show oxygen isotope compositions similar to chondrules in carbonaceous chondrites that compose the middle-to-outer asteroid belt. The presence of the chondrulelike objects in the comet suggests that chondrules have been transported out to the cold outer solar nebula and spread widely over the early solar system.

Many small particles were recovered from the Jupiter-family short-period comet 81P/Wild 2 by the Stardust mission (*1*). The particles are thought to represent dust that was present in the outer regions of the early solar system where Kuiper belt objects, the predecessor of short-period comets, presumably formed. The comet Wild 2, now orbiting between Mars and Jupiter, had a wider orbit reaching the Kuiper belt [30 to 50 astronomical units (AU) from the Sun] before 1974 (*2*). Asteroids are principally located much closer (3 to 5 AU) to the Sun and are presumed to be the parent bodies of the primitive class of meteorites, chondrites. These are mostly [up to 80% (*3*, *4*)] made up of chondrules, which were formed in the solar nebula around 4.565 billion years ago (*5*) by multiple episodes of total or partial melting of preexisting solid particles typically smaller than 1 mm in diameter. Here, we

[1]Department of Earth and Planetary Science, Faculty of Science, Kyushu University, Hakozaki, Fukuoka 812-8581, Japan. [2]College of Science, Ibaraki University, 2-1-1 Bunkyo, Mito 310-8512, Japan. [3]Department of Earth and Space Science, Graduate School of Science, Osaka University, Toyonaka 560-0043, Japan. [4]Department of Geology and Geophysics, University of Wisconsin-Madison, Madison, WI 53706–1692, USA. [5]Astromaterials Research and Exploration Science, NASA Johnson Space Center, Houston, TX 77058, USA. [6]Japan Synchrotron Radiation Research Institute, SPring-8, Sayo, Hyogo 679-5198, Japan. [7]Geological Survey of Japan, Advanced Industrial Science and Technology, Tsukuba 305-8567, Japan.

*To whom correspondence should be addressed. E-mail: tomoki@geo.kyushu-u.ac.jp
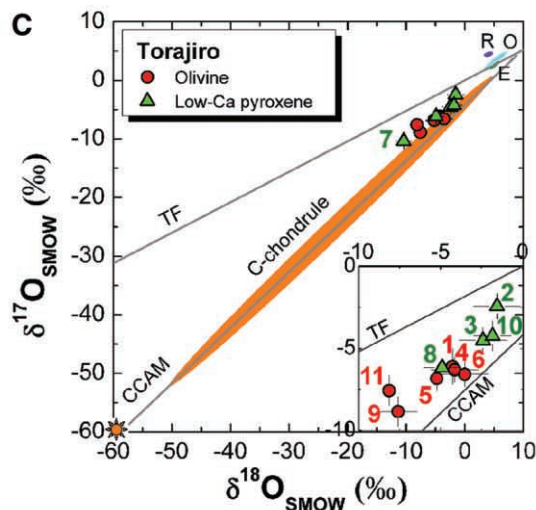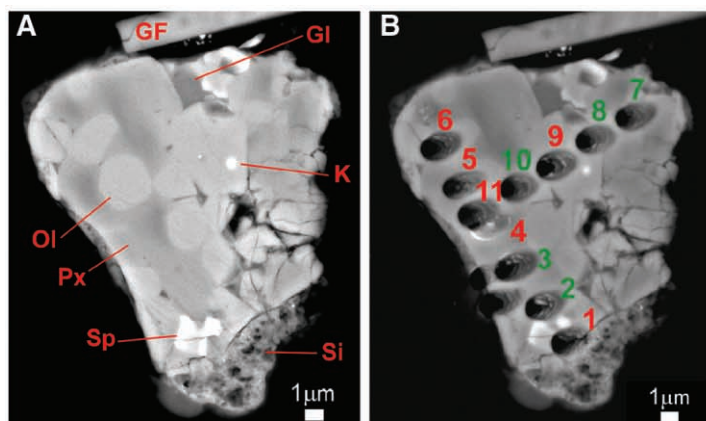
Fig. 1. Mineralogical, textural, and isotopic features of Torajiro. (**A**) Back-scattered electron (BSE) image of a cross section showing a porphyritic texture. Vesiculate melted aerogel is present with a sharp contact with Torajiro, indicating that Torajiro itself was not melted during the hypervelocity impact into aerogel. Gl, glass; K, kamacite; Ol, olivine; Px, low-Ca pyroxene; Sp, Cr-spinel; Si, silica aerogel; and GF, glass fiber holding the particle. (**B**) BSE image showing spots analyzed with ion microprobe for oxygen isotope ratios. We made two sets of line analysis at 3-μm intervals by using a small Cs$^+$ beam 2 μm in diameter. (**C**) Oxygen isotope ratios of olivine and low-Ca pyroxene. The data point numbers correspond to those in (B). Compositional fields of chondrules in various chondrites, including enstatite (E) (*17*), ordinary (O) (*15*), and rumuruti (R) (*16*); carbonaceous (C) (*19*, *20*) chondrites are also shown for comparison. The Sun symbol indicates the oxygen composition of the Sun (*31*). TF, terrestrial fractionation line; CCAM, carbonaceous chondrite anhydrous mixing line. Error bars represent ±2 SD.

report that the Stardust samples include chondrule-like objects. Fifty particles from comet Wild 2 were first analyzed by synchrotron radiation x-ray diffraction and microtomography to identify crystalline particles that retain original characteristics of cometary dust (6). Four particles, named Torajiro, Gozen-sama, Gen-chan, and Lilly, were chosen for detailed analysis (7).

Torajiro (C2054,0,35,6) is a terminal particle extracted from a small branch of track 35 (7). Electron microscopy (EM) of the polished surface shows a porphyritic texture (Fig. 1A) that consists mainly of olivine [Fo_{79-80} (see table S1 for chemical composition)], low-Ca pyroxene [$En_{86}Wo_3 \sim En_{79}Wo_5$ (table S1)], small kamacite blebs, and mesostasis glass enriched in SiO_2 and Al_2O_3 (table S1). O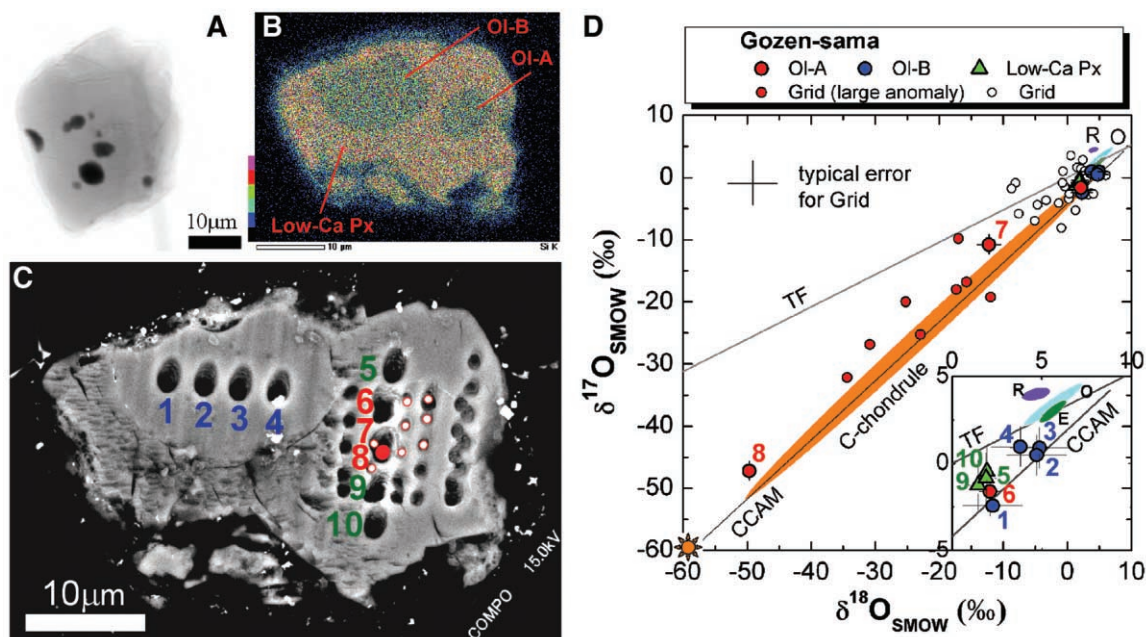n one side, olivine grains are poikilitically enclosed within pyroxene. Subhedral Cr-rich spinels are in contact with olivine. Ion-microprobe analysis (11 points as shown in Fig. 1B) indicates that Torajiro is heterogeneous in oxygen isotopic ratios (Fig. 1C). Olivine grains have a $\delta^{18}O$ relative to standard mean ocean water ($\delta^{18}O_{SMOW}$) of −8 to −4 per mil (‰). Low-Ca pyroxene, with slightly high Al_2O_3 and CaO contents (spot 7 in table S1), has a $\delta^{18}O$ of −10‰, whereas other pyroxenes (table S1) have a higher $\delta^{18}O$ of −5 to −2‰.

Gozen-sama (C2081,1,108,1) is the largest terminal particle (40 μm in diameter) in track 108 (7). Tomographic analysis shows that this particle contains many small round FeNi metal inclusions (Fig. 2A). EM of the polished surface indicates that it has a poikilitic texture (Fig. 2B); two rounded olivines (Ol-A and Ol-B) are enclosed within low-Ca pyroxene. Both grains are uniformly Fo_{95} (table S1). Low-Ca pyroxene is $En_{95}Wo_1$ (table S1) and monoclinic (7).

The oxygen isotope ratios of the crystals in Gozen-sama (10 points shown in Fig. 2C) are heterogeneous (Fig. 2D). Ol-A has the lowest $\delta^{18}O$ and varies from −50 to 2‰, whereas Ol-B has a higher $\delta^{18}O$, from 2 to 5‰. The low-Ca pyroxene has a composition intermediate between the two olivines. Analyses with a smaller primary beam (36 points shown in Fig. 2D and fig. S6) revealed that Ol-A contains a 3-μm-by-5-μm core area highly enriched in ^{16}O ($\delta^{18}O < −10‰$) (Fig. 2D and table S2), whereas the $\delta^{18}O$ of the rim is close to that of the surrounding low-Ca clinopyroxene.

Fig. 2. A large terminal particle, Gozen-sama, 40 μm in diameter. (**A**) Transmitted x-ray image showing that the particle contains many rounded dark inclusions of FeNi metal. The presence of a crescent-shaped inclusion on the far-left-hand side of the particle suggests ablation of the surface layers during capture. (**B**) Silicon x-ray map of a cross section showing a typical poikilitic fabric, in which two olivine phenocrysts (Ol-A and Ol-B) are contained within a low-Ca pyroxene oikocryst (low-Ca Px). (B) is rotated 90° counterclockwise relative to (A). (**C**) BSE image of the cross section in the same frame as (B), showing 10 2-μm diameter spots (numbered, average precision is ±1.3‰, 2 SD) and 36 smaller less precise 1-μm small spots (average precision is ±4.1‰, 2 SD) by ion microprobe. The 2-μm spot with a solid red dot shows the most negative oxygen anomaly, and 1-μm spots with outlined red marks show a surrounding large anomaly. (**D**) Oxygen isotope ratios obtained from 2-μm spots (numbered large marks) and 1-μm spots (small marks). The small red marks are data from the outlined red marks in (C). The star symbol indicates the oxygen isotopic composition of the Sun (31). Error bars represent ±2 SD.
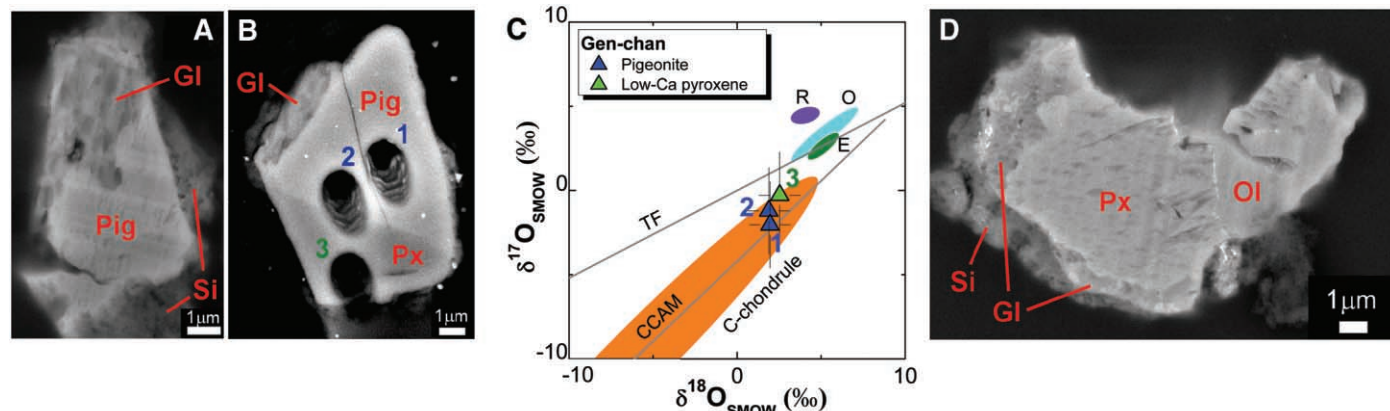
Fig. 3. (**A**) BSE image of a cross section of Gen-chan. (**B**) BSE image of another cross section of Gen-chan, wherein three spots analyzed for oxygen composition are shown. (**C**) Oxygen isotope ratios of pyroxenes in Gen-chan. The numbers correspond to those in (B). (**D**) BSE image of a cross section of Lilly. The thin white line between olivine and pyroxene is chromite. Gl, glass; Ol, olivine; Px, low-Ca pyroxene; Pig, pigeonite; Si, silica aerogel. Error bars represent ±2 SD.

Gen-chan (C2081,1,108,7) is a terminal particle of track 108. Observation of the polished surface shows Mn-rich pigeonite [$En_{84}Wo_{11}$ (table S1)], low-Ca pyroxene [$En_{97}Wo_2$ (table S1)], and SiO_2- and Al_2O_3-rich glass (Fig. 3, A and B, and table S1). The corroded shape of the pigeonite suggests resorption during partial melting or crystallization as hopper crystals. Oxygen isotope ratios in the pyroxenes are almost nearly constant (Fig. 3C).

Lilly (C2054,0,35,4) was located on the wall of track 35, close to Torajiro. It contains a large low-Ca pyroxene [$En_{89}Wo_4$ (table S1)] in contact with Mn-rich olivine [Fo_{91} and 2.0 weight percent (wt %) MnO (table S1)] and SiO_2- and Al_2O_3-rich glass or possibly albitic plagioclase (Fig. 3D). Submicroscopic chromite grains smaller than 100 nm in size are entrained at the boundary between pyroxene and olivine. We did not perform ion-microprobe analysis on this particle because it was difficult to polish.

Most chondrules in meteorites are characterized by (i) igneous porphyritic or poikilitic textures suggestive of partial melting at high temperatures; (ii) presence of glass formed during rapid cooling, which is directly in contact to silicates; and (iii) dominant occurrence of Mg-rich olivine and low-Ca pyroxene with minor amounts of rounded Fe-metal inclusions (3, 4), suggestive of crystallization under reducing conditions in space. These characteristics are observed in the four particles from Comet Wild 2. Therefore, these particles are chondrulelike objects formed by short-duration partial melting. The high abundance of low-Ca pyroxene sets them apart from other high-temperature objects, such as calcium aluminum–rich inclusions (CAIs) (3) and amoeboid olivine aggregates (8).

Before capture, the particles had been larger than the present size because they were ablated and disaggregated during deceleration in the aerogel (9). The entrance-hole sizes of impact tracks 35 and 108 [1.0 mm by 1.5 mm and 0.35 mm by 0.55 mm, respectively (fig. S3)] give an upper limit for the size of the initial incoming particles. It is uncertain whether any two particles from the same track (Gozen-sama and Gen-chan from track 108 and Torajiro and Lilly from track 35) were parts of a single chondrule before their capture, but the idea cannot be ruled out because Gozen-sama and Gen-chan contain low-Ca pyroxene with a similar Fe/Mg ratio (table S1). Compared with average meteorite porphyritic chondrules (3, 4), the crystal size of olivine in Torajiro and Gozen-sama [mostly 2 to 10 μm (Figs. 1A and 2B)] is much smaller. But some chondrites, such as the ALH-85085 CH chondrite, have similarly fine-grained chondrules (10).

In Torajiro and Gozen-sama, olivine and pyroxene have heterogeneous oxygen composition along the slope 1 line (Figs. 1C and 2D). Therefore, they should have formed through partial melting of precursor materials with various oxygen compositions. This is clearly seen in Gozen-sama, in which Ol-A and Ol-B show an extremely different $\delta^{18}O$, whereas pyroxene shows a homogeneous $\delta^{18}O$ intermediate between the two

olivines (Fig. 2D), indicating that olivine grains are partial-melting residue and that pyroxene crystallized from the melt. During heating, the Fe/Mg ratios of Ol-A and Ol-B almost equilibrated (table S1), but the oxygen isotope heterogeneity was preserved because oxygen diffusion in olivine (11) is much slower than Fe-Mg exchange in olivine (12). The extreme heterogeneity of oxygen isotope ratios in Gozen-sama may indicate spatial and temporal differences in the nebular-gas composition from which precursor olivine grains formed (13). After heating, Gozen-sama cooled rapidly; otherwise, the low-Ca pyroxene would not be monoclinic (14).

Major element abundances of olivine, pyroxene, and mesostasis glass in the four cometary particles (table S1) are within the range of compositions defined by a majority of meteorite chondrules (3, 4). However, the range of oxygen isotope ratios of these particles spans the entire range observed for chondrules in carbonaceous chondrites (Figs. 1C, 2D, and 3C). None of the data plots on or above the terrestrial mass fractionation line, which clearly resolves these particles from ordinary (15) and rumuruti (16) chondrite ($\Delta^{17}O = >0‰$) and enstatite (17) chondrite ($\Delta^{17}O = 0‰$) objects. Therefore, the chondrulelike objects in Wild 2 are most similar to type-I and -II olivine-pyroxene chondrules in carbonaceous chondrites. Spectroscopic studies infer that carbonaceous chondrites came from asteroids located mainly at the mid- to outer asteroid belt, whereas ordinary and enstatite chondrites are from the inner asteroid belt (18). Therefore, the Wild 2 chondrulelike objects have a strong relation with chondrules in the outer asteroid belt.

One notable difference from known carbonaceous chondrite chondrules is the extremely ^{16}O-rich sample, Gozen-sama (table S1). Most meteorite chondrules show a more limited range ($\delta^{18}O > -15‰$) (19) with few exceptions (down to $-51‰$ in $\delta^{18}O$) (20). Furthermore, MnO concentrations in some olivines [0.8 wt % in Torajiro and 2.0 wt % in Lilly (table S1)] and pyroxenes [0.6 wt % in Torajiro and 5.1 wt % in Gen-chan (table S1)] in Wild 2 chondrulelike objects are higher than those in meteorite chondrules [lower than 0.5 wt % in most cases (3)]. Although the origin of MnO enrichment is not clear (21), it is commonly observed in Wild 2 olivine and pyroxene (22).

Our study demonstrates that chondrulelike objects were present at Kuiper belt–formation regions. These objects may be present in the other studied Wild 2 particles based on the presence of roeddorite, a characteristic mineral of alkali-rich chondrules (23), and Si-O-Al–rich glass in contact to pyroxene (24). The presence of both chondrulelike objects and CAIs (25) in Wild 2 suggests that high-temperature components of short-period comets and asteroids are similar.

The gas density in the protoplanetary disk decreased with distance from the Sun (26). In situ production of chondrules in the Kuiper belt region by shock-wave propagation would require a gas

density much higher than that envisaged by standard solar nebular models (27). Otherwise, the temperature of preexisting solid dust precursors would not reach the melting point (27). Therefore, formation of chondrules directly in the Kuiper belt is unlikely.

Similarities in oxygen isotope ratios between cometary chondrulelike objects and asteroidal chondrules suggest that chondrules formed in the inner solar nebula and were transported to the outer nebula by an X-wind (28) or outward flow in the midplane (29). The CAI particle called Inti (1) contains (Ti, V)N (30), the highest temperature condensate from a gas with solar composition, which also requires the material transportation across the solar nebula. The most ^{16}O-rich composition of Wild 2 chondrulelike objects is $-49.7 \pm 0.9‰$ in $\delta^{18}O$ (table S1) and that of the Wild 2 CAI (25) is $-41.6 \pm 1.3‰$ in $\delta^{18}O$, suggesting that both sampled a common oxygen reservoir during formation, probably from an inner solar nebula with the same oxygen composition as the Sun (31).

References and Notes
1. D. Brownlee *et al.*, *Science* **314**, 1711 (2006).
2. M. Królikowska, S. Szutowicz, *Astron. Astrophys.* **448**, 401 (2006).
3. A. J. Brearley, R. H. Jones, in *Planetary Materials*, J. J. Papike, Ed. (Mineralogical Society of America, Chantilly, VA, 1998), chap. 3, pp. 1–398.
4. J. N. Grossman, A. E. Rubin, H. Nagahara, E. A. King, in *Meteorites and the Early Solar System*, J. F. Kerridge, M. S. Matthews, Eds. (Univ. Arizona Press, Tucson, AZ, 1988), pp. 619–659.
5. Y. Amelin, A. N. Krot, I. D. Hutcheon, A. A. Ulyanov, *Science* **297**, 1678 (2002).
6. T. Nakamura *et al.*, *Meteorit. Planet. Sci.* **43**, 247 (2008).
7. Materials and methods are available as supporting material on *Science* Online.
8. L. J. Chizmadia, A. Rubin, J. T. Wasson, *Meteorit. Planet. Sci.* **37**, 1781 (2002).
9. G. J. Flynn *et al.*, *Science* **314**, 1731 (2006).
10. J. N. Grossman, A. E. Rubin, G. J. MacPherson, *Earth Planet. Sci. Lett.* **91**, 33 (1988).
11. O. Gérard, J. Jaoul, *J. Geophys. Res.* **94**, 4119 (1989).
12. R. Dohmen, T. Chakraborty, *Phys. Chem. Miner.* **34**, 409 (2007).
13. J. Aléon, A. El Goresy, E. Zinner, *Earth Planet. Sci. Lett.* **263**, 114 (2007).
14. J. R. Smyth, *Am. Mineral.* **59**, 345 (1974).
15. R. N. Clayton, T. K. Mayeda, J. N. Goswami, E. J. Olsen, *Geochim. Cosmochim. Acta* **55**, 2317 (1991).
16. M. K. Weisberg *et al.*, *Geochim. Cosmochim. Acta* **55**, 2657 (1991).
17. R. N. Clayton, T. K. Mayeda, *Proc. Lunar Planet. Sci. Conf.* **XVI**, 142 (1985).
18. M. J. Gaffey, J. F. Bell, D. P. Cruikshank, in *Asteroid II*, R. P. Binzel, T. Gehrels, M. S. Matthews, Eds. (Univ. Arizona Press, Tucson, AZ, 1989), pp. 98–127.
19. R. N. Clayton, *Annu. Rev. Earth Planet. Sci.* **21**, 115 (1993).
20. R. H. Jones *et al.*, *Geochim. Cosmochim. Acta* **68**, 3423 (2004).
21. W. Klöck, K. L. Thomas, D. S. Mckay, H. Palme, *Nature* **339**, 126 (1989).
22. M. E. Zolensky *et al.*, *Science* **314**, 1735 (2006).
23. D. J. Joswiak *et al.*, *38th Lunar Planet. Sci. Conf.* abstract 2142; www.lpi.usra.edu/meetings/lpsc2007/pdf/2142.pdf (2007).
24. K. Tomeoka, N. Tomioka, I. Ohnishi, *Meteorit. Planet. Sci.* **43**, 273 (2008).
25. K. D. McKeegan *et al.*, *Science* **314**, 1724 (2006).
26. C. Hayashi, K. Nakazawa, Y. Nakagawa, in *Protostars and Planets II*, D. C. Black, M. S. Matthews, Eds. (Univ. Arizona Press, Tucson, AZ, 1985), pp. 1100–1153.

27. A. Iida, T. Nakamoto, H. Susa, *Icarus* **153**, 430 (2001).
28. F. H. Shu, H. Shang, A. E. Glassgold, T. Lee, *Science* **277**, 1475 (1997).
29. F. J. Ciesla, *Science* **318**, 613 (2007).
30. D. E. Brownlee *et al.*, *39th Lunar Planet. Sci. Conf.* abstract 1978; www.lpi.usra.edu/meetings/lpsc2008/pdf/1978.pdf (2008).
31. K. D. McKeegan *et al.*, *39th Lunar Planet. Sci. Conf.* abstract 2020; www.lpi.usra.edu/meetings/lpsc2008/pdf/2020.pdf (2008).

Political Attitudes Vary with Physiological Traits

Douglas R. Oxley,[1]* Kevin B. Smith,[1]* John R. Alford,[2] Matthew V. Hibbing,[3] Jennifer L. Miller,[1] Mario Scalora,[4] Peter K. Hatemi,[5] John R. Hibbing[1]†

Although political views have been thought to arise largely from individuals' experiences, recent research suggests that they may have a biological basis. We present evidence that variations in political attitudes correlate with physiological traits. In a group of 46 adult participants with strong political beliefs, individuals with measurably lower physical sensitivities to sudden noises and threatening visual images were more likely to support foreign aid, liberal immigration policies, pacifism, and gun control, whereas individuals displaying measurably higher physiological reactions to those same stimuli were more likely to favor defense spending, capital punishment, patriotism, and the Iraq War. Thus, the degree to which individuals are physiologically responsive to threat appears to indicate the degree to which they advocate policies that protect the existing social structure from both external (outgroup) and internal (norm-violator) threats.

The nature and source of political attitudes have been the subject of much study (*1–3*). Traditionally, such attitudes were believed to be built from sensible, unencumbered reactions to environmental events (*4*), but more recent research emphasizes the built-in, almost "automated" quality of many political responses (*5*), which has been suggested to be based in brain activation variations in limbic regions (*6–8*). The research task is now to determine why some people seem primed to adopt certain political attitudes, whereas others appear primed to adopt quite different attitudes. For example, although images and reminders of the terrorist attacks of 9-11 produce an aggregate shift in political views (*9, 10*), the reasons for individual variability in the degree of attitudinal shifts are unknown.
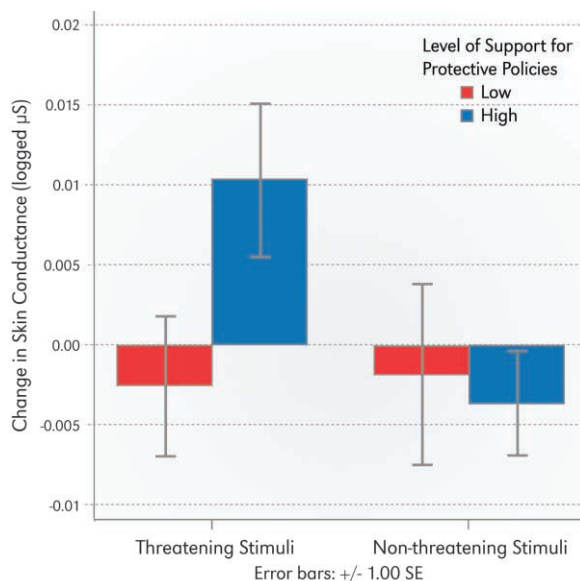
One possibility is that people vary in general physiology and that certain of these variations encourage the adoption of particular political attitudes. Broad, physiologically relevant traits such as feelings of disgust and fear of disease have been suggested to be related to political attitudes (*11, 12*), and political beliefs can be predicted by observing brain activation patterns in

response to unanticipated events, such as one letter of the alphabet appearing on a computer screen when the respondent expected a different letter (*13*). A connection between self-reports of felt threat and political attitudes has also been identified in previous research (*14–19*).

The physiology of response to a perceived threat is an attractive topic of investigation because an appropriate response to environmental threat is necessary for long-term survival and because perceived threat produces a variety of reasonably well-mapped, physically instantiated responses (*20*). If the threat is abrupt, a defensive cascade of linked, rapid extensor-flexor movement occurs

throughout the body within 30 to 50 ms (*21*), presumably to reduce vital-organ vulnerability (e.g., eye blink and retraction of the head). Less immediately, perceived threat causes signals from the sensory cortex to be relayed to the thalamus and ultimately to the brain stem, resulting in heightened noradrenergic activity in the locus ceruleus (*22*). Acetylcholine, acting primarily through the amygdala but also through the hypothalamic-pituitary-adrenal axis (*23*), stimulates release of epinephrine, which in turn leads to activation of the sympathetic division of the autonomic nervous system. Though these basic response patterns apply in all people, individual sensitivity to perceived threat varies widely (*24*).

To test the hypothesis that variations in physical sensitivity to threat are associated with political beliefs, in May 2007, we conducted a random telephone sample of the population of Lincoln, Nebraska. Participants were screened [see supporting online material (SOM)] to identify those with strong political attitudes (regardless of the content of those attitudes), and qualifying individuals were invited to a lab in the city. During the first visit, the 46 participants completed a survey instrument (see SOM) ascertaining their political beliefs, personality traits, and demographic characteristics. During the second session, about 2 months after the first, participants were attached to physiological equipment, making it possible to measure skin conductance and orbicularis oculi startle blink electromyogram (EMG) response (*25*).

[1]Department of Political Science, University of Nebraska-Lincoln, Lincoln, NE 68588, USA. [2]Department of Political Science, Rice University, Houston, TX 77251, USA. [3]Department of Political Science, University of Illinois, Urbana-Champaign, Urbana, IL 61801, USA. [4]Department of Psychology, University of Nebraska-Lincoln, Lincoln, NE 68588, USA. [5]Virginia Institute for Psychiatric and Behavioral Genetics, Richmond, VA 23298, USA.

*These authors contributed equally to this work.
†To whom correspondence should be addressed. E-mail: jhibbing@unl.edu

Fig. 1. Changes in skin conductance (in microsiemens) resulting from the viewing of threatening and nonthreatening images for high supporters and low supporters of socially protective policies. Difference of means tests: threatening stimuli $t = 1.98$, $P = 0.05$; nonthreatening stimuli $t = 0.284$, $P = 0.77$, two-tailed tests. All skin conductance data have been logged. Support for policies is measured by self-reported positions on 18 issues relevant to group life (see text), with "high support" including those participants above the median of support and "low support" including those participants below the median.

1667

Science

Chondrulelike Objects in Short-Period Comet 81P/Wild 2

Tomoki Nakamura, Takaaki Noguchi, Akira Tsuchiyama, Takayuki Ushikubo, Noriko T. Kita, John W. Valley, Michael E.
Zolensky, Yuki Kakazu, Kanako Sakamoto, Etsuko Mashio, Kentaro Uesugi and Tsukasa Nakano

ARTICLE TOOLS	http://science.sciencemag.org/content/321/5896/1664
SUPPLEMENTARY MATERIALS	http://science.sciencemag.org/content/suppl/2008/09/18/321.5896.1664.DC1 http://science.sciencemag.org/content/suppl/2008/09/18/321.5896.1664.DC2
RELATED CONTENT	http://science.sciencemag.org/content/sci/321/5896/1699.2.full file:/contentpending:yes
REFERENCES	This article cites 23 articles, 7 of which you can access for free http://science.sciencemag.org/content/321/5896/1664#BIBL
PERMISSIONS	http://www.sciencemag.org/help/reprints-and-permissions

Use of this article is subject to the Terms of Service